

Numerical calculations of spectral turnover and Synchrotron Self Absorption in CSS and GPS radio sources.

S. Jeyakumar^{*}

Departamento de Astronomía, Universidad de Guanajuato, AP 144, Guanajuato CP 36000, México.

ABSTRACT

The dependence of the turnover frequency on the linear size is presented for a sample of GPS and CSS radio sources derived from complete samples. The dependence of the luminosity of the emission at the peak frequency with the linear size and the peak frequency is also presented for the galaxies in the sample. The luminosity of the smaller sources evolve strongly with the linear size. Optical depth effects have been included to the 3D model for the radio source of Kaiser (2000) to study the spectral turnover. Using this model, the observed trend can be explained by synchrotron self absorption. The observed trend in the peak-frequency – linear-size plane is not affected by the luminosity evolution of the sources.

Key words: radiation mechanisms: non-thermal – galaxies: active – radio continuum: galaxies

1 INTRODUCTION

The current consensus is that the Compact Steep Spectrum (CSS) and Giga-hertz Peaked Spectrum (GPS) sources are young radio sources, evolving in the Inter-Stellar Medium (ISM) of the host galaxy (cf. Fanti et al. 1995; Carvalho 1998; O’Dea 1998; Murgia et al. 1999; Jeyakumar et al. 2005). These classes of radio sources provide the opportunity to study the evolution of the radio sources in their youth and the interaction of the radio jets and lobes with the material in the ISM. The GPSs are selected based on the turnover in the spectrum. Although the CSSs are not selected based on such a turnover, the spectra of most of the CSSs show either a turnover or flattening at very low frequencies (Fanti et al. 1990). The processes that can produce turnover in the spectrum are synchrotron self-absorption (SSA), free-free absorption (FFA) and Induced Compton Scattering (ICS) (O’Dea & Baum 1997; Bicknell et al. 1997; Kuncic et al. 1998). Studies of a few individual sources report evidence of FFA in them (Bicknell et al. 1997; Xie et al. 2005; Kamenno et al. 2003b,a). Mutoh et al. (2002) find that the polarisation properties are not according to the trend expected from SSA. However using a sample of GPS galaxies Snellen et al. (2000) find that the turnover is consistent with SSA.

The intrinsic turnover frequency (ν_{peak}) is found to be anti-correlated with the linear size (LS) of the source, in

the complete samples of CSS and GPS sources (O’Dea & Baum 1997, hereafter OB97; Fanti et al. 1990). It has been shown that FFA by the material ionised by the fast moving cocoon of the young radio source can explain this trend (Bicknell et al. 1997). Alternatively, using a model for the evolution of the source O’Dea & Baum (1997) could predict such an anti-correlation using a simple homogeneous SSA model. However the observed trend is flatter than that predicted by SSA. This could be due to the evolution of the luminosity of the radio source resulting in the observed trend (O’Dea & Baum 1997) or due to the picture of SSA by a homogeneous medium being too simple. So, in this work a 3D model is used to study the effects of the evolution of the radio source on the observed trend in the ν_{peak} – LS plane, in the context of SSA. New samples of GPS and CSS sources have become available in recent years which have been used to extend the ν_{peak} – LS plane. In addition, the luminosity evolution of the sources is also studied. The sample of sources is described in Section 2. The SSA model and the model results are described in Sections 3 and 4 respectively. A summary of the results is presented in Section 5.

2 THE SAMPLE OF SOURCES

The sample of sources is derived from the complete samples of CSS and GPS sources available in the literature. The GPS sources have well defined turnover in the spectrum by selection. The CSS sources are selected based on the spec-

* E-mail: sjkastro.ugto.mx

tral index and is not necessary to have a turnover in the spectrum. Since the aim here is to study the turnover in the spectrum, only those CSS sources with a clear turnover or flattening of the spectrum at low frequencies are considered here. In the case of flattening of the spectrum at low frequencies, the measurement at the lowest available frequency is chosen as the turnover frequency. Those CSSs, mostly from the B3-VLA CSS sample, which show a curvature at low frequencies without a clear flattening are also not considered here (Fanti et al. 2001). Variability studies of the GPS sources have shown that most of the quasars identified as GPSs may not be genuine peakers, but flaring blazars (Tinti et al. 2005; Tinti & De Zotti 2005; Tornikoski et al. 2001). To avoid such sources affecting the results, only those GPS catalogues for which structural information is available for most of the sources are considered. However galaxies from the GPS catalogues are considered to study the dependence of the ν_{peak} with L_{peak} (luminosity at the peak frequency) even if the structural information is not available (cf. Tinti et al. 2005). The samples of CSS and GPS sources used here are described below.

(C) The Fanti et al. (1990) sample of CSSs from the 3C catalogue. The sources in this sample which do not follow the above criteria are, 3C43, 3C186, 3C190, 3C303.1, 3C305.1 and 3C455. These sources have been removed from the current sample.

(S) The Stanghellini et al. (1998) sample of GPSs. These two samples are well studied. The sources from these samples are listed in O’Dea & Baum (1997).

(F) The B3-VLA sample of CSS sources (Fanti et al. 2001). Information on the structure of the sources is available for most of the sources (Dallacasa et al. 2002a,b).

(W) The sample of GPS galaxies from the WENSS catalogue (Snellen et al. 2000).

(A) The sample of CSS and GPS sources in the southern sky (Edwards & Tingay 2004). From this sample only those galaxies listed in Tinti & De Zotti (2005) are considered.

(P) The sample of confirmed CSOs (Peck & Taylor 2000; Gugliucci et al. 2005) are also used for this study irrespective of the liberal selection criteria on the spectral index, since the CSOs are known to be young radio sources (Readhead et al. 1996; Owsianik & Conway 1998; Gugliucci et al. 2005). In this sample, some of the sources show flat spectra (see below) making it difficult to estimate the turnover frequencies. Such sources have been removed from the current sample.

(D) The galaxies from the sample of High Frequency Peakers (Dallacasa et al. 2000) listed in Tinti & De Zotti (2005).

(H) The sample of GPS galaxies from the Parkes half-Jy catalogue (Snellen et al. 2002).

(B) The galaxies from the Bolton et al. (2004) sample of GPS sources listed in Tinti & De Zotti (2005).

(L) The GPSs from the CORALZ sample (Snellen et al. 2004).

For the sources in the samples (C), (P) and (F) the flux density measurements available in the literature (from NED and the CATS database) have been used to fit the spectrum as described in Steppe et al. (1995). The values of ν_{peak} and S_{peak} (flux density at the peak frequency) estimated from this fit are listed in the tables.

Of these samples (H), (B) and (L) have been used to study only the dependence of ν_{peak} with L_{peak} , since infor-

Table 1. The sample of GPS galaxies

Source	Sample ^a	z^b	ν_{peak}^c MHz	S_{peak} Jy	$\log(L_{peak})$ W/Hz/Sr
J0020+3152	B	1.1*	4910	0.0438	25.29
J0032+2758	B	0.51*	4600	0.0344	24.33
J0936+3207	B	0.20*	14000	0.056	23.62
J1506+4239	B	0.38*	14000	0.766	25.38
J1517+3936	B	0.46*	21000	0.043	24.32
J1526+4201	B	0.36*	8100	0.067	24.27
J1530+3758	B	0.19*	3430	0.141	23.97
J1540+4138	B	0.17*	8800	0.046	23.38
J1550+4536	B	0.50*	3500	0.062	24.57
J1554+4350	B	1.2*	10900	0.045	25.40
J0108–1201	H	1.0*	1000	0.9	26.49
J0206–3024	H	0.65*	500	0.9	26.01
J0210+0419	H	1.5*	400	1.3	27.14
J0210–2213	H	1.4*	1500	1.1	26.98
J0242–2132	H	0.314	1000	1.3	25.42
J0323+0534	H	0.37*	400	7.1	26.32
J0401–2921	H	0.65*	400	1	26.05
J0407–3924	H	0.54*	400	1.4	26.00
J0407–2757	H	0.68*	1500	1.4	26.25
J0433–0229	H	0.36*	400	3	25.92
J0441–3340	H	0.65*	1500	1.2	26.13
J0457–0848	H	0.52*	400	1	25.82
J0913+1454	H	0.47*	600	1.1	25.75
J1044–2712	H	0.65*	1500	0.8	25.96
J1057+0012	H	0.65*	400	1.6	26.26
J1109+1043	H	0.55*	500	2.4	26.25
J1110–1858	H	0.497	1000	0.9	25.72
J1122–2742	H	0.65*	1400	0.8	25.96
J1135–0021	H	0.16*	400	2.9	25.12
J1203+0414	H	0.33*	400	1.4	25.50
J1345–3015	H	0.65*	400	2.5	26.45
J1350–2204	H	0.63*	400	1.4	26.17
J1352+0232	H	0.47*	400	2	26.01
J1352+1107	H	0.65*	400	3.6	26.61
J1447–3409	H	0.65*	500	1	26.05
J1506–0919	H	0.43*	600	1.6	25.82
J1548–1213	H	0.883	400	3.7	26.96
J1556–0622	H	0.94*	400	2.4	26.84
J1600–0037	H		1000	1.2	27.10
J1604–2223	H	0.141	600	1	24.54
J1640+1220	H	1.150	400	3.7	27.27
J1648+0242	H	0.65*	400	3.4	26.58
J2058+0540	H	1.381	400	3.1	27.41
J2123–0112	H	1.158	400	2	27.01
J2151+0552	H	0.740	5000	1.2	26.27
J2325–0344	H	1.4*	1400	1.2	27.02
J2339–0604	H	1.2*	400	3.8	27.33
J0733+5605	L	0.104	460	0.42	23.88
J0739+4954	L	0.054	950	0.1	22.67
J0831+4608	L	0.127	2200	0.13	23.56
J0906+4636	L	0.085	680	0.3	23.56
J1317+4115	L	0.066	2300	0.27	23.28
J1718+5441	L	0.147	480	0.44	24.22

^a See text for the meaning of the labels in the sample column.

^b The * denotes a photometric redshift. ^c Here ν_{peak} refers to the observed value

mation on the source structure is not available for the majority of the sources. The sources from these three samples are listed in Table 1. The columns are arranged as follows: column 1: source name; column 2: master sample; column 3: redshift ; column 4: observed ν_{peak} in MHz ; column 5: S_{peak} in Jy; column 6: log of L_{peak} in W/Hz/Sr. The sources from all other samples are listed in Table 2. The columns are arranged as follows: column 1: source name; column 2: master sample; column 3: optical id; column 4: redshift ; column 5: largest angular size (LAS) in arc seconds; column 6: observed ν_{peak} in MHz ; column 7: S_{peak} in Jy; column 8: log of L_{peak} in W/Hz/Sr ; column 9: references to LAS, ν_{peak} and S_{peak} . Sources appearing on many samples are counted only once. A redshift of 1.5 is assumed for those sources without any redshift measurement. The cosmological constants used here are, $H_0 = 75 \text{ kms}^{-1}\text{Mpc}^{-1}$ and $q_0=0.0$.

Other samples of CSS and GPS sources available in the literature are, the CSS sources from the FIRST catalogue (Kunert et al. 2002), the weak CSSs (Tschager et al. 2003), the B2 sample of CSSs (Saikia et al. 2002), the sample of CSSs from the S4 sample (Saikia et al. 2001) and the sample of GPSs from the JVAS sample (Marecki et al. 1999). Since the optical identification or structural information is less complete in these catalogues, they are not considered here.

The combined sample consists of a total of 203 sources of which 150 are CSS/GPS sources and 53 are GPS galaxies. The sample size used in the present study is about three times larger than OB97 sample of sources. The upper ranges of redshift, linear size and peak luminosity are similar in both the samples. There are only three sources with large rest frame peak frequency in the current sample. The lowest redshift in this sample is 0.004 as compared to 0.08 in the OB97 sample. However the present sample extends the range of linear sizes by an order of magnitude lower to about 0.65 pc and the peak luminosity by 2.5 orders of magnitude lower than the OB97 sample.

3 MODEL FOR SPECTRAL TURNOVER

It is well known that SSA can produce turnover in the spectrum. The ν_{peak} occurs at a frequency where the SSA optical depth becomes unity. The SSA optical depth, $\tau_{SSA} = \alpha_\nu R$, where R is the path length through the source and α_ν is the synchrotron self absorption coefficient which is given in Eqn. 2. The τ_{SSA} depends on the electron number density, the magnetic field and the path length, which all vary as the source evolves. Thus a model for the evolution of the radio source is required to understand the evolution of ν_{peak} with LS .

In the recent years, semi-analytical models of dynamical and spectral evolution of classical radio sources have been constructed (Kaiser & Alexander 1997, hereafter KA; Kaiser, Dennett-Thorpe & Alexander 1997, hereafter KDA; Kaiser 2000, hereafter K00; Blundell et al. 1999; Manolakou & Kirk 2002), based on self-similarity (Falle 1991). These models provide a very useful tool to study the evolution of radio emission from the radio sources evolving in a power-law ambient medium. Of these models, K00 provide a method of constructing the 3-dimensional emissivity of the cocoon (see also Chyzy 1997).

Here, 3-dimensional synchrotron self-absorption coeffi-

cient, α_ν , has been constructed using the approach of K00. This has been used to evolve the radio spectrum with the age of the source, including synchrotron self absorption. The method employed here and the parameters involved are described below.

The radio source with jet power, Q_0 evolves in an ambient medium of density $\rho(L_j) = \rho_0 a_0^\beta L_j^{-\beta}$, where L_j is the length of the jet. The explicit expressions for the length L_j is given by KA. The synchrotron emissivity of a small volume element which was injected into the cocoon at time t_i and has evolved to the present time t , can be written as

$$\epsilon(\nu, t, t_i) = \frac{c\sigma_T}{6\pi\nu} \gamma(t)^3 u_b(t, t_i) n(\gamma, t, t_i) \quad (1)$$

where $u_b(t, t_i)$ is the energy density of the magnetic field and $n(\gamma, t, t_i)$ is the electron energy spectrum. The synchrotron self absorption coefficient is,

$$\alpha_\nu = K_0 n_0 B^{(p+2)/2} \nu^{-(p+4)/2} \quad (2)$$

where K_0 is a constant (Shu 1991). The scaling factor $n_0 = n(\gamma, t, t_i)/\gamma^{-p}$, where p is the power-law energy index of the electrons. The lower and upper bound of the γ factor at injection are γ_{min} and γ_{max} respectively.

The equations for quantities u_b , $n(\gamma)$ injected at time t_i and their evolution to the present time t are given in KDA. In order to construct a 3D model, K00 uses a specialised geometry for the cocoon and assume that the volume element injected at time t_i is located at l (in units of L_j) as a thin cylindrical volume of thickness δl and radius $r_c(l, \alpha_1, \alpha_2)$ (equation 12 of K00). The location of the cylindrical volume element l is given by $(t_i/t)^{\alpha_3}$. Since all the δl have to add up to the length of the jet, the constant α_3 can be calculated self consistently for the assumed geometry parameters α_1 and α_2 , using the equation 15 of K00.

Using the above approach, ϵ_ν and α_ν are obtained at the position (l, y) , where y is the perpendicular distance from the jet axis. These quantities are assumed to be axisymmetric with respect to the jet axis. If the source is viewed edge-on, the path length for a ray passing through the position (l, y) is, $R(l, y) = 2\sqrt{(r_c(l))^2 - y^2}$ and $r_c(l)$ is the cocoon radius at l . The surface brightness, including the optical depth effects, along this ray can be written as,

$$S_\nu(l, y) = \frac{\epsilon(\nu, l, y)}{\alpha(\nu, l, y)} \{1 - \exp[-\alpha(\nu, l, y)R(l, y)]\} \quad (3)$$

The total emission from the cocoon, obtained by integrating over the surface, is given by

$$P_\nu = 4 \int_{l_{low}}^1 L_j(t) dl \int_0^{r_c(l)} S_\nu(l, y) dy \quad (4)$$

Here l_{low} depends on whether that part of the cocoon can have electrons with γ corresponding to the given frequency, had that value at injection been γ_{max} .

In the model of KA, the jet length has to be large enough to allow for the pressure balance between the cocoon and the jet that passed through the re-confinement shock. For a source size of 10 pc and $\beta = 1.9$ the ratio of the location of the re-confinement shock to the length of the jet, R_{conf} , is about 0.1. Thus the jet length is much larger than the location of the re-confinement shock and the model results can be applied to such sources. However, the density at the inner region of the host galaxy is not expected to vary as steeply as in the outer regions. A realistic situation is a

Table 2. The sample of CSS & GPS sources[†]

Source	Sample ^a	ID	z^b	LAS "	ν_{peak}^c MHz	S_{peak} Jy	LS kpc	$\log(L_{peak})$ W/Hz/Sr	Ref ^d
J0022+0014	SH	G	0.305	0.06	700	3.47	0.24	25.82	1,20
J0111+3906	SP	G	0.669	0.006	4000	1.33	0.0373	26.21	1,20
J0137+3309	C	Q	0.367	0.5	80	68.6	2.25	27.29	1
J0141+1353	C	G	0.621	0.92	100	10.8	5.53	27.04	1
J0224+2750	C	G	0.309	2.5	26	21	10.1	26.61	1
J0226+3421	C	Q	2.910	1.1	150	4.4	9.97	28.53	1,20
J0240-2309	S	Q	2.223	0.018	1000	7.05	0.158	28.37	1
J0251+4315	S	Q	1.316	0.06	5000	1.27	0.473	26.96	1,20
J0318+1628	SC	G	0.3	800	9.55	2.44	28.00	1,20	1,20
J0321+1221	C	Q	2.662	0.02	400	2.4	0.179	28.15	1
J0348+3353	C	G	0.244	0.25	40	21	0.858	26.38	1
J0410+7656	CP	G	0.5985	0.15	350	6.9	0.885	26.80	1
J0431+2037	SC	G	0.219	0.25	1100	4.02	0.793	25.56	1,20
J0432+4138	C	G	1.023	0.08	150	18	0.586	27.82	1
J0459+0229	S	Q	2.384	0.012	2100	1.89	0.106	27.90	1,16,20
J0503+0203	SH	Q	0.583	0.015	1800	2.51	0.0874	26.34	1,20
J0521+1638	C	Q	0.760	0.60	200	18.7	3.94	27.50	1
J0542+4951	C	Q	0.545	0.55	100	69.4	3.1	27.71	1
J0713+4349	SP	G	0.518	0.025	1900	2.09	0.137	26.13	1,20
J0741+3112	S	Q	0.630	0.010	5300	3.82	0.0605	26.60	1,20
J0745+1011	S	G	2.624	0.010	2700	4.12	0.0896	28.36	1,20
J0745-0044	S	Q	0.994	0.005	5800	2.12	0.0363	26.85	1,20
J0943-0819	SH	G	0.228	0.05	500	3.4	0.163	25.52	1,20
J1008+0730	C	G	0.877	1.3	16	45.5	9.03	28.04	1
J1021+2159	C	G	1.617	0.84	80	17	6.96	28.35	1
J1035+5628	SP	Q	0.459	0.040	1300	1.87	0.206	25.96	1,20
J1120+1420	SH	G	0.362	0.08	500	3.89	0.358	26.03	1,20
J1130-1449	S	Q	1.187	0.003	1000	5.8	0.023	27.50	1,20
J1146-2447	S	Q	1.950	0.006	2200	1.69	0.0515	27.58	1,20
J1156+3128	C	Q	1.557	0.9	150	8.2	7.39	27.98	1
J1206+6413	C	G	0.371	1.36	90	15.3	6.17	26.65	1
J1227+3635	C	Q	1.974	0.060	900	2.2	0.516	27.71	1
J1248-1959	S	Q	1.280	0.50	500	8.69	3.92	27.77	1,20
J1252+5634	C	Q	0.321	1.67	40	13	6.91	26.44	1
J1326+3154	SC	G	0.369	0.06	500	7.03	0.271	26.31	1,20
J1330+2509	C	Q	1.055	0.048	40	28	0.355	28.04	1
J1331+3030	C	Q	0.849	3.2	80	35	22	27.89	1
J1347+1217	SH	G	0.122	0.080	400	8.86	0.16	25.35	1,20
J1400+6210	SCP	G	0.429	0.07	500	6.56	0.346	26.43	1,20
J1407+2827	SD	G	0.077	0.007	4200	2.76	0.00936	24.43	1,20
J1416+3444	C	EF		0.06	700	2.1	0.489	27.34	1
J1419+0628	C	Q	1.439	1.49	60	82	12	28.88	1
J1445+0958	SC	Q	3.535	0.02	900	2.61	0.184	28.58	1,20
J1459+7140	C	Q	0.905	2.11	40	40.3	14.8	28.03	1
J1520+2016	C	G	0.752	1.05	40	23	6.86	27.57	1
J1521+0430	SH	S	1.296	0.135	800	4.58	1.06	27.50	1,20
J1602+3326	SC	G	1.100	0.06	2400	3.06	0.45	27.13	1,20
J1609+2641	SC	G	0.473	0.05	1100	5.44	0.261	26.45	1,20
J1634+6245	C	Q	0.988	0.20	150	14.1	1.45	27.67	1
J1638+6234	C	G	0.75	0.24	150	14.2	1.57	27.36	1
J1821+3942	C	G	0.4	0.44	250	7.7	2.09	26.43	1
J1831+2907	C	Q	0.842	3.1	74	7.57	21.2	27.22	1
J2011-0644	SH	G	0.547	0.030	1400	2.64	0.169	26.29	1,20
J2129-1538	S	Q	3.27	0.008	4100	1.23	0.0733	28.14	1,20
J2130+0502	SH	G	0.990	0.030	700	4.93	0.217	27.22	1,20
J2136+0041	S	Q	1.936	0.002	4300	8.59	0.0171	28.28	1,20
J2212+0152	SH	G		0.055	500	4.51	0.448	27.68	1,20
J2250+7129	C	G	1.841	1.6	40	13	13.6	28.39	1
J2251+1848	C	Q	1.758	0.66	40	30	5.56	28.70	1
J2344+8226	SC	Q	0.735	0.18	500	6.29	1.17	26.99	1,20
J2355+4950	SP	G	0.237	0.050	700	2.93	0.168	25.50	1,20

Table 2. continued

Source	Sample ^a	ID	z^b	LAS "	ν_{peak}^c MHz	S_{peak} Jy	LS kpc	$\log(L_{peak})$ W/Hz/Sr	Ref ^d
J0003+4807	P	EF		0.011	2123	0.348	0.0896	26.56	4
J0132+5620	P	EF		0.012	3437	0.6	0.0977	26.80	4
J0204+0903	P	EF		0.029	1061	1.96	0.236	27.31	4
J0427+4133	P	EF		0.0067	3416	0.823	0.0546	26.94	5
J0620+2102	P	EF		0.027	1308	0.86	0.22	26.96	4
J0650+6001	P	Q	0.455	0.00642	4977	0.88	0.0328	25.62	6
J0753+4231	P	Q	3.59	0.00892	952	0.727	0.0824	28.05	7
J0754+5324	P	EF		0.0203	1240	0.634	0.165	26.82	4
J1111+1955	P	G	0.299	0.018	1305	1.1	0.0711	25.30	4
J1148+5924	P	G	0.011	0.0205	6149	0.573	0.0043	22.03	8
J1357+4353	P	G			2146	0.551		26.76	4
J1414+4554	P	G	0.19	0.030	693	0.396	0.0855	24.42	4
J1546+0026	PH	G	0.55	0.0083	365	2.28	0.047	26.23	4
J1734+0926	PH	G	0.61*	0.015	1622	1.05	0.0893	26.01	4,16
J1815+6127	P	Q	0.601	0.0101	645	0.824	0.0597	25.88	7
J1816+3457	P	G	0.245	0.037	440	0.983	0.127	25.05	4
J1823+7938	P	G	0.224	0.0156	7039	0.554	0.0503	24.72	7
J1845+3541	P	G	0.764	0.0208	2545	1.07	0.137	26.26	17
J1944+5448	P	G	0.263	0.041	778	1.77	0.148	25.38	6
J2022+6136	P	Q	0.2280	0.0077	4086	2.64	0.0251	25.41	18
J2203+1007	P	EF		0.010	4427	0.306	0.0814	26.51	4
J0000+4054	FP	E		0.12	323	2.06	0.977	27.33	3,21
J0042+3739	F	G	1.006	0.12	333	2.4	0.874	26.92	3,21
J0042+4009	F	E		3.7	74	4.04	30.1	27.63	3
J0225+4229	F	G	3.5*	3.4	151	1.83	31.3	28.41	3
J0704+3911	F	Q	1.238	1.8	151	1.7	14	27.02	3
J0706+4647	F	E		0.075	777	1.81	0.611	27.28	3,21
J0725+3917	F	E		0.30	280	3.26	2.44	27.53	3,22
J0758+3929	F	G	2.119	2.6	151	3.2	22.6	27.97	3
J0804+4704	F	E		1.0	151	3.6	8.14	27.58	3
J0812+4019	F	G	0.551	1.2	151	3.47	6.8	26.42	3
J0825+3919	F	G	1.18	0.07	517	1.77	0.536	26.98	3,21
J0843+4215	F	E		0.135	412	2.13	1.1	27.35	3,21
J0958+3848	F	E		4.8	74	2.44	39.1	27.41	3
J1010+4159	F	E		0.265	116	1.5	2.16	27.20	3,21
J1011+4204	F	E		0.115	424	1.16	0.937	27.08	3,21
J1017+3901	F	G	0.206	6.1	74	7.08	18.5	25.75	3
J1019+4408	F	G	0.33*	0.155	342	1.17	0.653	25.42	3,21
J1030+3857	F	E		1.6	107	1.28	13	27.13	3
J1047+4508	F	G	4.1*	1.0	209	2.32	9.32	28.74	3
J1052+3811	F	G	1.018	0.21	429	1.33	1.54	26.68	3,21
J1058+4010	F	E		2.8	74	2.78	22.8	27.47	3
J1131+4514	F	G	0.4	0.5	151	6.3	2.37	26.34	3
J1135+4258	F	E		0.045	1044	1.41	0.367	27.17	3,21
J1139+3803	F	E		0.07	335	0.891	0.57	26.97	3,21
J1143+4621	F	G	0.06	8.1	151	5.46	8.64	24.50	3
J1200+4548	F	G	0.742	0.62	258	2.89	4.03	26.66	3,22
J1201+3919	F	G	2.37	0.07	467	0.934	0.619	27.58	3,21
J1204+3912	F	G	0.445	2.1	74	1.94	10.6	25.94	3
J1207+3954	F	G	2.066	1.6	74	3.39	13.9	27.96	3
J1214+3748	F	G	1.5*	0.47	74	3.42	3.83	27.56	3,22
J1227+4400	F	G	0.22*	0.42	103	1.68	1.34	25.18	3,21
J1244+4048	FP	Q	0.811	0.07	405	2.03	0.472	26.60	3,21
J1343+4343	F	E		0.13	338	1.22	1.06	27.11	3,21
J1345+3823	F	Q	1.844	0.13	412	1.72	1.1	27.52	3,21
J1434+4236	F	E		0.05	74	1.67	0.407	27.24	3,21
J1442+4044	F	E		0.13	292	1.55	1.06	27.21	3,21
J1451+4154	F	E		0.12	296	2.19	0.977	27.36	3,21
J2303+4439	F	G	1.7*	0.5	74	7.05	4.18	28.03	3,22
J2304+4028	F	E		0.6	151	3.74	4.89	27.59	3
J2307+3802	F	G	0.4*	0.15	151	2.72	0.712	25.98	3,21

Table 2. continued

Source	Sample ^a	ID	z^b	LAS "	ν_{peak}^c MHz	S_{peak} Jy	LS kpc	$\log(L_{peak})$ W/Hz/Sr	Ref ^d
J2332+4030	F	E		0.10	162	2.13	0.814	27.35	3,21
J0404+6050	W	G		0.0044	1000	0.184	0.0358	26.29	9
J0440+6157	W	G		0.0171	1000	0.237	0.139	26.40	9
J0541+6745	W	G	1.5*	0.0040	5700	0.192	0.0326	26.30	9
J0544+6201	W	G	1.4*	0.0061	1900	0.129	0.0489	26.05	9
J0834+5803	W	G	0.093	<0.0043	1600	0.065	0.00679	22.97	9
J1525+6751	W	G	1.1*	0.0224	1800	0.163	0.168	25.86	9
J1552+6813	W	G	1.3*	0.0025	1500	0.052	0.0197	25.56	9
J1557+6211	W	G	0.9*	<0.0044	2300	0.049	0.0308	25.10	9
J1600+7123	W	G		0.0227	1700	0.346	0.185	26.56	9
J1623+6624	W	G	0.201	<0.0029	4000	0.363	0.00862	24.43	9
J1655+6441	W	G		0.0248	1000	0.069	0.202	25.86	9
J1841+6718	W	G	0.486	0.0061	2100	0.178	0.0324	25.00	9
J1941+7221	W	G	1.1*	0.0315	1400	0.233	0.236	26.01	9
J1945+7055	WP	G	0.101	0.0319	1800	0.929	0.0541	24.20	9
J0241-0815	A	G	0.004	0.041	7500	2.71	0.00316	21.82	10,12
J1543-0757	AH	G	0.172	0.050	700	1.65	0.132	24.94	10
J1658-0739	A	G		0.007	4800	1.32	0.057	27.14	10
J1723-6500	A	G	0.014	0.007	2700	4.48	0.00186	23.13	10,14
J1726-6427	A	G			1100	3.96		27.62	10
J1744-5144	A	G		0.052	1000	6.94	0.424	27.86	10
J1939-6342	A	G	0.183	0.042	1400	15	0.116	25.96	10
J2257-3627	A	G	0.006	<0.100	2700	1.37	0.0115	21.88	10,13
J2336-5236	A	G			1100	1.97		27.32	10
J0428+3259	D	G	0.3		7300	0.545		24.99	23
J0655+4100	D	G	0.02156	0.0016	7800	0.33	0.000648	22.38	23,11,19
J1511+0518	D	G	0.084	0.0049	11100	0.778	0.00708	23.96	23,15
J1735+5049	D	G		0.00336	6400	0.972	0.0274	27.01	23,6

† A machine readable version of this table is available in CDS. ^a See text for the meaning of the labels in the sample column. ^b The * denotes a photometric redshift. ^c Here ν_{peak} refers to the observed value. ^d The references are: (1) O’Dea (1998); (2) Taylor & Vermeulen (1997); (3) Fanti et al. (2001); (4) Peck & Taylor (2000); (5) Gugliucci et al. (2005); (6) Xu et al. (1995); (7) Taylor et al. (1994); (8) Taylor et al. (1998); (9) Snellen et al. (2000); (10) Edwards & Tingay (2004); (11) Henstock et al. (1995); (12) Kamenon et al. (2001); (13) Tingay et al. (2003); (14) Ojha et al. (2004); (15) Xiang et al. (2002); (16) Stanghellini et al. (1999); (17) Polatidis et al. (1995); (18) Kellermann et al. (1998); (19) Dallacasa et al. (2000); (20) Stanghellini et al. (1998); (21) Dallacasa et al. (2002a); (22) Dallacasa et al. (2002b); (23) Tinti et al. (2005);

King type profile with a constant density core. The models with shallower density profile $\beta \sim 0.0$ are a good representation for the smaller sources. For R_{conf} of about 0.3 and β of 0.0 and 0.5 the size of the source is about 150 and 50 pc respectively. Therefore at smaller sizes the model results are to be treated as extrapolation of the trend at larger sizes.

Alexander (2000) has presented a method of switching from one power-law model to another that can apply to evolution from smaller to larger sources and has shown that the luminosity from different models match very close to the point of switching. It turns out that the location where the pressure from different models match is same as the location where the analytical luminosities of Alexander (2000) match. So model results are also considered by switching from $\beta = 0$ model to $\beta = \beta_{outer}$ at the distance where the pressure of the cocoon of different power-law models match. For $\beta_{outer} = 1.9$, the pressures match at $L_j = 1.22 a_0$. Although, all the quantities involved in estimating the luminosity of the source are related to the pressure, the continuity of the evolutionary tracks in the $\nu_{peak} - L_{peak}$ or the $\nu_{peak} - LS$ plane is not guaranteed. In addition, the evolutionary

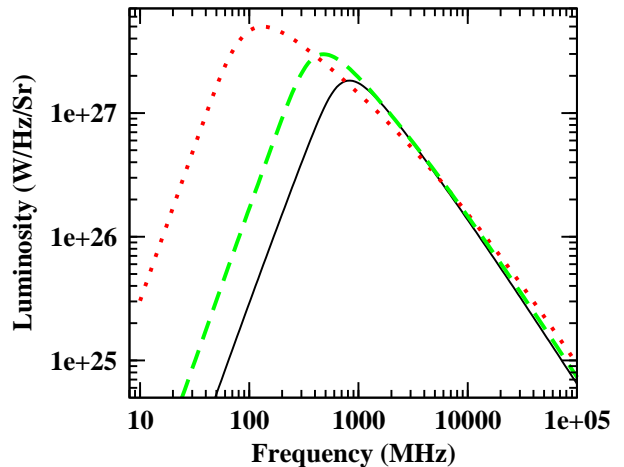


Figure 1. The model spectra for radio sources of sizes 1 (solid), 2 (dashed) and 10 (dotted) kpc are plotted. The parameters used for the model calculations are $Q_0 = 0.13 \times 10^{40}$, $a_0 = 2$ kpc and $\beta = 1.9$.

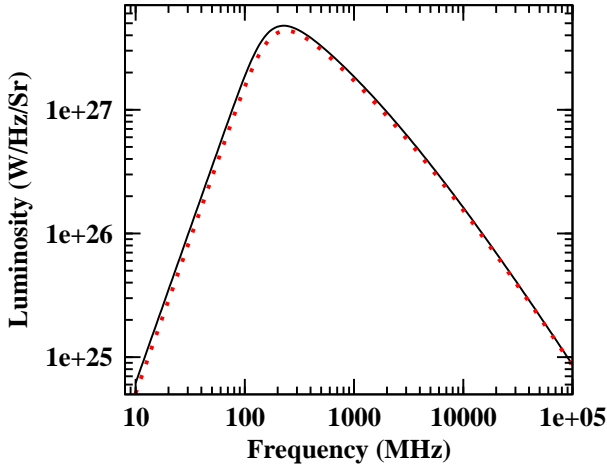


Figure 2. The model spectra for a source with linear size of 4.88 kpc. The solid line represents the model with $\beta = 0$ and the dotted line represents $\beta = 1.9$. The parameters used for the model calculations are as in Fig. 1.

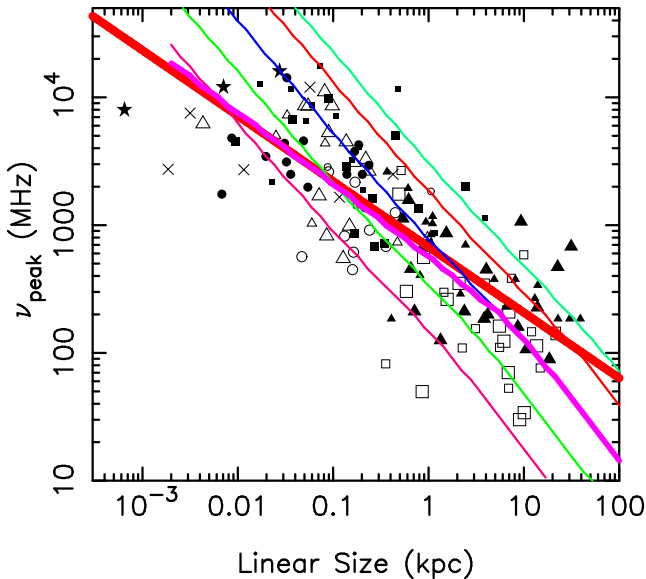


Figure 3. The ν_{peak} , is plotted against the linear size of the radio source. The symbols representing the samples are: unfilled square – C; filled square – S; unfilled triangle – P; filled triangle – F; unfilled circle – H; filled circle – W; unfilled star L; filled star – D; plus – B; cross – A. The quasars are plotted with symbol sizes smaller than that of the galaxies. The thick solid line represents the least squares fit to the data. The thin lines from the bottom to the top of the figure represent models with $Q_0 = 1.3 \times 10^{37}$, 1.3×10^{38} , 1.3×10^{39} , 1.3×10^{40} and 5×10^{50} W respectively. The model with $\beta = 0$ at the inner core and $\beta = 1.9$ at the outer regions is plotted with a line of intermediate thickness.

history of the energy of the electrons of the two power-law models are different. However it can be seen from Fig. 2 that indeed the luminosity and the ν_{peak} are very close to each other at the switching point, but not exactly the same. Results obtained using this approach are also presented in the next section.

4 RESULTS

The model spectrum is obtained by numerically integrating Eqn. 4. The geometry parameters used in the model calculations are, $\alpha_1 = 2$ and $\alpha_2 = 1/3$. A very high value is chosen for γ_{max} and $\gamma_{min} = 1.0$. In addition, the value of the hotspot to the cocoon pressure is taken as $4R_T^2$, where $R_T = 2$. Other parameters assumed for the model calculations correspond to the case-2 of KDA. The model spectrum is presented in Fig. 1, for a radio source of size 1, 2 and 10 kpc for $\beta = 1.9$. The figure shows that the ν_{peak} shifts to low frequencies as the source grows in size. The spectral index at the optically thick side of the spectrum is about $5/2$. The point at which the pressure of the cocoon of the models with $\beta = 0$ and 1.9 match, corresponds to a source size of 4.88 kpc. The model spectrum for a source with this size is presented for $\beta = 0$ and 1.9 in Fig. 2. This figure shows that the spectra from the two different power-law models are indeed close to each other.

4.1 Dependence of ν_{peak} with LS

The value of ν_{peak} is plotted against the LS in Fig. 3, for the quasars and the galaxies from the combined sample listed in Table 2. The meaning of the different symbols are explained in the caption. A linear fit to all the data gives a slope of -0.51 ± 0.03 , which is shown as thick solid line in the figure. A linear fit to only the galaxies give a slope of -0.50 ± 0.04 . The slope obtained with the new sample is somewhat flatter than the slope of -0.65 ± 0.05 obtained by O’Dea & Baum (1997).

The same dependence calculated using the current model is also plotted in Fig. 3 for jet powers of, 1×10^{37} , 1.3×10^{38} , 1.3×10^{39} , 1.3×10^{40} and 5×10^{40} W. These curves fit the data well. The slope of the model curves for $\beta = 1.9$, is about -0.85 . For $\beta = 0$ the slope of the model curve is -0.56 which is close to the linear fit to the observed data. These results suggest that SSA can explain the turnover in the spectrum and the observed trend in $\nu_{peak} - LS$ plane can be explained by SSA alone. The sources evolve from GPS to CSS in the $\nu_{peak} - LS$ plane and do not leave this plane during the evolution. However large CSS sources with low jet power may not show turnover in the observable frequency range and may leave this plane during the later stages of evolution.

Using the radio source model of Begelman (1996) and assumption on the variation of the magnetic field, B, O’Dea & Baum (1997) predict a slope from -1.65 to -1.8 depending on their model parameters. The is steeper than that given by this model. Interestingly the slope predicted by (Bicknell et al. 1997) for the case of FFA, for $\beta = 1.9$ is about -0.91 . This is very similar to the slope predicted by the current model with $\beta = 1.9$. For $\beta = 0.0$, the current model prediction fits the observed trend well. It is not possible to favour any one mechanism from this slope alone. However, if both mechanisms are at work, then the spectral index on the optically thick side is expected to be steeper than that predicted by either of the mechanisms. Although in general this is not the case, it is interesting observationally. Detailed modelling of the spectrum of high resolution observations of a few GPS sources suggest that both mechanisms could be at work (Xie et al. 2005; Kameno et al. 2003b,a).

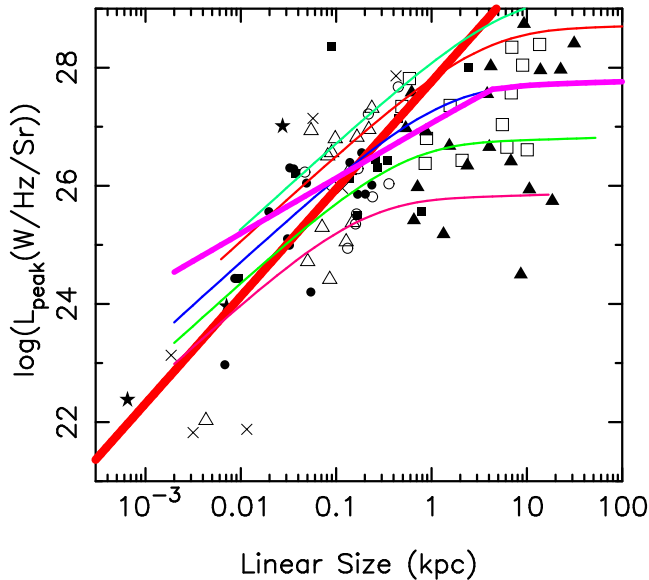


Figure 4. The L_{peak} is plotted against the LS for the galaxies from Tables 1 and 2. The meaning of the symbols and the line types are as in Fig. 3.

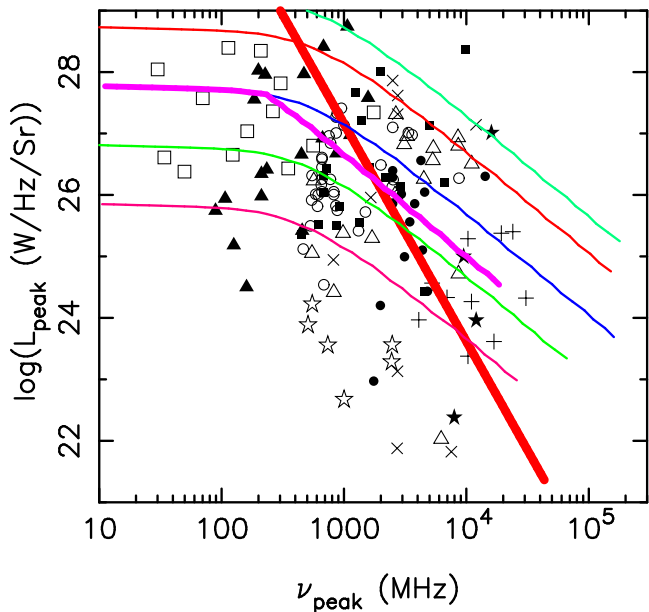


Figure 5. The L_{peak} is plotted against the ν_{peak} for the galaxies from Tables 2 and 1. The meaning of the symbols and the line types are as in Fig. 3.

4.2 Luminosity evolution

The value of L_{peak} is plotted against the LS in Fig. 4. for sources from Table 1. Since the luminosities of the quasars are affected by the beaming effects, only galaxies are plotted in the above diagram. The figure shows that the L_{peak} increases with the LS for the sources with sizes less than about 1 kpc. Beyond this size the L_{peak} does not vary with LS. A parabolic fit to the data (not shown here) clearly shows a flattening at large sizes. A linear least squares fit to the data for $\log(\text{LS})$ smaller than -0.5 is shown as thick solid line. The

slope of the fit is 1.8 ± 0.2 . The results from the model are also plotted in the figure for the same parameters used in the above section. The slope of the model curves at smaller linear sizes for $Q_0 = 1.3 \times 10^{39}$ W and β of 0 and 1.9 are 0.94 and 1.41 respectively. The slope is higher for higher jet powers. This trend is also consistent with the prediction of Snellen et al. (2000). Although the trend shown by the model curves are in agreement with the observed trend, the observations suggest a steeper evolution than the model prediction.

It is possible to study this luminosity evolution in the $L_{peak} - \nu_{peak}$ plane, where all the GPSs without angular size estimates can be used. This will increase the number of sources with very high frequencies or correspondingly small linear sizes. The dependence of L_{peak} with ν_{peak} is shown in Fig. 5 for all the galaxies. The figure shows a trend of L_{peak} decreasing with ν_{peak} . The relations $\nu_{peak} \propto \text{LS}^{-0.51}$ and $L_{peak} \propto \text{LS}^{1.8}$ obtained from the least squares fits above can be translated to $L_{peak} \propto \nu_{peak}^{-3.5}$. This trend is shown as a thick solid line. Such a trend is expected for a power-law electron energy spectrum since the γ of the electrons corresponding to the ν_{peak} is higher and the electron density is lower for higher γ values. However the slope expected from this argument is the spectral index α which is smaller than the least squares fit. The curves of the model results are plotted for the same parameters used for the model curves in Fig. 3. The model curves show that the peak luminosity decreases with increasing ν_{peak} for values of $\nu_{peak} > \nu_{cut}$. The value of ν_{cut} is the turnover frequency expected for a source size of about 1 kpc. For smaller ν_{peak} values corresponding to larger sources the L_{peak} is almost constant. The slope of the model curves for $\beta = 1.9$ and 0 is -1.58 and -1.67 respectively. This reflects the same trend seen in the $L_{peak} - \text{LS}$ plane. Most of the sources in this diagram can be bound by curves corresponding to jet powers between 1.3×10^{37} and 5×10^{40} W. The observed trend and the model curves suggest that the luminosity increases as the source evolves from GPS to CSS and it is unlikely to observationally miss the CSS sources due to evolution. However it is possible to miss the smaller GPSs since they will appear more fainter at the frequencies away from the ν_{peak} . These missing sources do not affect the trend seen in Fig. 3.

5 CONCLUSIONS

The dependence of ν_{peak} with linear size is presented for the CSS and GPS sources derived from complete samples available in the literature. The ν_{peak} is anti-correlated with the linear size, as $\nu_{peak} \propto \text{LS}^{-0.51}$ for this sample. The sources evolve in luminosity as they grow in linear size. The L_{peak} increases with the LS of the source for sizes smaller than about 0.3 kpc, as $L_{peak} \propto \text{LS}^{1.8}$. Beyond this size the L_{peak} is almost constant. This luminosity evolution is seen in the $L_{peak} - \nu_{peak}$ plane also. Optical depth effect has been included to the 3D model of K00. Using this model the observed dependence of the ν_{peak} with linear size and L_{peak} can be explained. These results suggest that synchrotron self absorption can explain the turnover in the young radio sources. The luminosity evolution does not affect the trend seen in the $\nu_{peak} - \text{LS}$ plane.

ACKNOWLEDGMENTS

Critical comments and suggestions made by the anonymous referee, which have helped in refining the interpretation and also improving the presentation are acknowledged. SJ thanks Paul J. Wiita for useful comments on the paper. This research has made use of the NASA/IPAC Extragalactic Database (NED) which is operated by the Jet Propulsion Laboratory, California Institute of Technology, under contract with the National Aeronautics and Space Administration. The authors made use of the database, CATS (Verkhodanov et al. 1997) of the Special Astrophysical Observatory. This work was partially supported by PROMEP/103-5/07/2462 and Conacyt CB-2009-01/130523 grants.

REFERENCES

- Alexander P., 2000, MNRAS, 319, 8
 Begelman M. C., 1996, Baby Cygnus A's. Cygnus A – Study of a Radio Galaxy, p. 209
 Bicknell G. V., Dopita M. A., O'Dea C. P. O., 1997, ApJ, 485, 112
 Blundell K. M., Rawlings S., Willott C. J., 1999, AJ, 117, 677
 Bolton R. C., Cotter G., Pooley G. G., Riley J. M., Waldram E. M., Chandler C. J., Mason B. S., Pearson T. J., Readhead A. C. S., 2004, MNRAS, 354, 485
 Carvalho J. C., 1998, A&A, 329, 845
 Chyzy K. T., 1997, MNRAS, 289, 355
 Dallacasa D., Fanti C., Giacintucci S., Stanghellini C., Fanti R., Gregorini L., Vigotti M., 2002, A&A, 389, 126
 Dallacasa D., Stanghellini C., Centonza M., Fanti R., 2000, A&A, 363, 887
 Dallacasa D., Tinti S., Fanti C., Fanti R., Gregorini L., Stanghellini C., Vigotti M., 2002, A&A, 389, 115
 Edwards P. G., Tingay S. J., 2004, A&A, 424, 91
 Falle S. A. E. G., 1991, MNRAS, 250, 581
 Fanti C., Fanti R., Dallacasa D., Schilizzi R. T., Spencer R. E., Stanghellini C., 1995, A&A, 302, 317
 Fanti C., Pozzi F., Dallacasa D., Fanti R., Gregorini L., Stanghellini C., Vigotti M., 2001, A&A, 369, 380
 Fanti R., Fanti C., Schilizzi R. T., Spencer R. E., Nan Rendong, Parma P., van Breugel W. J. M., Venturi T., 1990, A&A, 231, 333
 Gugliucci N. E., Taylor G. B., Peck A. B., Giroletti M., 2005, ApJ, 622, 136
 Henstock D. R., Browne I. W. A., Wilkinson P. N., Taylor G. B., Vermeulen R. C., Pearson T. J., Readhead A. C. S., 1995, ApJS, 100, 1
 Jeyakumar S., Wiita P. J., Saikia D. J., Hooda J. S., 2005, A&A, 432, 823
 Kaiser C. R., 2000, A&A, 362, 447
 Kaiser C. R., Alexander P., 1997, MNRAS, 286, 215
 Kaiser C. R., Dennett-Thorpe J., Alexander P., 1997, MNRAS, 292, 723
 Kameno S., Inoue M., Wajima K., Sawada-Satoh S., Shen Z.-Q., 2003a, Publications of the Astronomical Society of Australia, 20, 134
 Kameno S., Inoue M., Wajima K., Sawada-Satoh S., Shen Z.-Q., 2003b, Publications of the Astronomical Society of Australia, 20, 213
 Kameno S., Sawada-Satoh S., Inoue M., Shen Z.-Q., Wajima K., 2001, PASJ, 53, 169
 Kellermann K. I., Vermeulen R. C., Zensus J. A., Cohen M. H., 1998, AJ, 115, 1295
 Kuncic Z., Bicknell G. V., Dopita M. A., 1998, ApJL, 495, L35
 Kunert M., Marecki A., Spencer R. E., Kus A. J., Niezgoda J., 2002, A&A, 391, 47
 Manolakou K., Kirk J. G., 2002, A&A, 391, 127
 Marecki A., Falcke H., Niezgoda J., Garrington S. T., Patnaik A. R., 1999, A&AS, 135, 273
 Murgia M., Fanti C., Fanti R., Gregorini L., Klein U., Mack K.-H., Vigotti M., 1999, A&A, 345, 769
 Mutoh M., Inoue M., Kameno S., Asada K., Kenta F., Uchida Y., 2002, PASJ, 54, 131
 O'Dea C. P., 1998, PASP, 110, 493
 O'Dea C. P., Baum S. A., 1997, AJ, 113, 148
 Ojha R., Fey A. L., Johnston K. J., Jauncey D. L., Reynolds J. E., Tzioumis A. K., Quick J. F. H., Nicolson G. D., Ellingsen S. P., Dodson R. G., McCulloch P. M., 2004, AJ, 127, 3609
 Owsianik I., Conway J. E., 1998, A&A, 337, 69
 Peck A. B., Taylor G. B., 2000, ApJ, 534, 90
 Polatidis A. G., Wilkinson P. N., Xu W., Readhead A. C. S., Pearson T. J., Taylor G. B., Vermeulen R. C., 1995, ApJS, 98, 1
 Readhead A. C. S., Taylor G. B., Xu W., Pearson T. J., Wilkinson P. N., Polatidis A. G., 1996, ApJ, 460, 612
 Saikia D. J., Jeyakumar S., Salter C. J., Thomasson P., Spencer R. E., Mantovani F., 2001, MNRAS, 321, 37
 Saikia D. J., Thomasson P., Spencer R. E., Mantovani F., Salter C. J., Jeyakumar S., 2002, A&A, 391, 149
 Shu F. H., 1991, The physics of astrophysics: Radiation. Vol. 1, University Science Books, Mill Valley, California
 Snellen I. A. G., Lehnert M. D., Bremer M. N., Schilizzi R. T., 2002, MNRAS, 337, 981
 Snellen I. A. G., Mack K.-H., Schilizzi R. T., Tschager W., 2004, MNRAS, 348, 227
 Snellen I. A. G., Schilizzi R. T., Miley G. K., de Bruyn A. G., Bremer M. N., Röttgering H. J. A., 2000, MNRAS, 319, 445
 Stanghellini C., O'Dea C. P., Dallacasa D., Baum S. A., Fanti R., Fanti C., 1998, A&AS, 131, 303
 Stanghellini C., O'Dea C. P., Murphy D. W., 1999, A&AS, 134, 309
 Steppe H., Jeyakumar S., Saikia D. J., Salter C. J., 1995, A&AS, 113, 409
 Taylor G. B., Vermeulen R. C., 1997, ApJL, 485, L9
 Taylor G. B., Vermeulen R. C., Pearson T. J., Readhead A. C. S., Henstock D. R., Browne I. W. A., Wilkinson P. N., 1994, ApJS, 95, 345
 Taylor G. B., Wrobel J. M., Vermeulen R. C., 1998, ApJ, 498, 619
 Tingay S. J., Edwards P. G., Tzioumis A. K., 2003, MNRAS, 346, 327
 Tinti S., Dallacasa D., de Zotti G., Celotti A., Stanghellini C., 2005, A&A, 432, 31
 Tinti S., De Zotti G., 2005, ArXiv Astrophysics e-prints, arXiv:astro-ph/0509439
 Tornikoski M., Jussila I., Johansson P., Lainela M., Valtaoja E., 2001, AJ, 121, 1306
 Tschager W., Schilizzi R. T., Röttgering H. J. A., Snellen

- I. A. G., Miley G. K., Perley R. A., 2003, *A&A*, 402, 171
Verkhodanov O. V., Trushkin S. A., Andernach H., Cherenkov V. N., 1997, in *ASP Conf. Ser. 125: Astronomical Data Analysis Software and Systems VI The CATS Database to Operate with Astrophysical Catalogs*. p. 322
Xiang L., Stanghellini C., Dallacasa D., Haiyan Z., 2002, *A&A*, 385, 768
Xie G., Jiang D. R., Shen Z.-Q., 2005, *ApJL*, 621, L13
Xu W., Readhead A. C. S., Pearson T. J., Polatidis A. G., Wilkinson P. N., 1995, *ApJS*, 99, 297